Human Pharmacokinetic and Dosimetry Studies of [^{18}F]FHBG: A Reporter Probe for Imaging Herpes Simplex Virus Type-1 Thymidine Kinase Reporter Gene Expression

Shahriar Yaghoubi, Jorge R. Barrio, Magnus Dahlbom, Meera Iyer, Mohammad Namavari, Nagichettiar Satyamurthy, Robin Goldman, Harvey R. Herschman, Michael E. Phelps, and Sanjiv S. Gambhir

Crump Institute for Molecular Imaging, UCLA–DOE Laboratory of Structural Biology and Molecular Medicine; Department of Molecular and Medical Pharmacology, Division of Nuclear Medicine; Molecular Biology Institute; Department of Biomathematics; and Jonsson Comprehensive Cancer Center, UCLA School of Medicine, University of California, Los Angeles, California

9-[4-[^{18}F]fluoro-3-(hydroxymethyl)butyl]guanine ([^{18}F]FHBG) has been used as a reporter probe to image expression of herpes simplex virus type-1 thymidine kinase (HSV1-tk) reporter gene in living animals. Our aim was to study the kinetics, biodistribution, stability, dosimetry, and safety of [^{18}F]FHBG in healthy human volunteers, preparatory to imaging patients undergoing HSV1-tk gene therapy. **Methods:** [^{18}F]FHBG was synthesized with a specific activity of 37,000–444,000 GBq/mmol and a radiochemical purity $>$ 99%. Ten healthy volunteers consented to participate in the study. A transmission scan was obtained before bolus injection of 70.3–229.4 MBq [^{18}F]FHBG into a hand vein, followed by dynamic PET imaging with 4 consecutive emission scans. Warmed hand-vein blood was withdrawn at various times after injection for blood time–activity measurements. Electrocardiography, blood pressure, and blood and urine pharmacologic parameters were measured before and after injection of the [^{18}F]FHBG tracer (n = 5). The stability of [^{18}F]FHBG in the urine was analyzed. Attenuation-corrected images were reconstructed using the ordered-subsets expectation maximization algorithm. Image region-of-interest time–activity data were used with the MIRD program to estimate absorbed radiation dosages. **Results:** [^{18}F]FHBG had rapid blood clearance; only 8.42% ± 4.76% (mean ± SD) of the peak blood activity remained at approximately 30 min. The average ratio of plasma activity to whole-blood activity during the study was 0.91 ± 0.04. Penetration of [^{18}F]FHBG across the blood–brain barrier was not observed. The primary routes of clearance were renal and hepatobiliary. High activities were observed in the bladder, gut, liver, and kidneys, but $<$0.0002% of the injected dose per gram was observed in other tissues. In the urine, 83% of activity 180 min after injection was stable [^{18}F]FHBG. Blood and urine pharmacologic parameters did not change significantly after injection of the [^{18}F]FHBG tracer. The bladder absorbed the highest radiation dose. **Conclusion:** [^{18}F]FHBG has the desirable in vivo characteristics of stability, rapid blood clearance, low background signal, biosafety, and acceptable radiation dosimetry in humans. This study forms the foundation for using [^{18}F]FHBG in applications to monitor HSV1-tk reporter gene expression.

Key Words: 9-[4-[^{18}F]fluoro-3-(hydroxymethyl)butyl]guanine; dosimetry; PET; herpes simplex virus type-1 thymidine kinase

J Nucl Med 2001; 42:1225–1234

Herpes simplex virus type-1 thymidine kinase (HSV1-tk) is a commonly studied suicide gene for cancer gene therapy (*1*,*2*). The use of HSV1-tk gene therapy in animal models has led to many different clinical trials, including trials for glioma, mesothelioma, prostate cancer, leukemia, and lymphoma (*3*–*6*). In many of these trials, the HSV1-tk gene is introduced through a variety of gene vectors and then the pro-drug ganciclovir is administered intravenously to kill cells expressing the HSV1-tk gene, through termination of DNA synthesis. Many attempts have been made to specifically direct the expression of HSV1-tk gene to cancer cells (*7*–*9*). However, noninvasive imaging of HSV1-tk therapeutic gene expression in humans has not been reported. Imaging the biodistribution, magnitude, and time variation of HSV1-tk gene expression should enhance progress in suicide gene therapy of cancer.

HSV1-tk can also be used as a PET reporter gene (PRG) to follow the expression of other transgenes, such as therapeutic genes administered to patients during gene therapy (*10*–*12*). This use is made possible by linking the expression of the transgene and the PRG such that a direct correlation exists between their expressions. Bicistronic vectors may be constructed such that a single promoter regulates the transcription of a messenger RNA containing coding regions for both the transgene and the PRG. In such a construct, the coding region for the transgene and the coding region for the PRG are separated by an internal ribosomal entry site, leading to the production of a separate protein

Received Sep. 5, 2000; revision accepted Jan. 10, 2001.

For correspondence or reprints contact: Sanjiv S. Gambhir, MD, PhD, UCLA School of Medicine, 700 Westwood Plaza, A-222B CIMI, Los Angeles, CA 90095-1770.

from each coding region. Using this type of construct, a correlated linkage between the expression of 2 PRGs has been shown in vivo with micro-PET (*13*). The transgene and PRG may also be introduced together on separate vectors but with the same promoter sequence (*14*).

Considering the foreseeable wide utility of PRGs, we set out to analyze the feasibility of using a high-affinity PET reporter probe (PRP) clinically. PRPs for HSV1-tk include acycloguanosines and uracil analogs. Imaging HSV1-tk expression with the uracil nucleoside derivative 5-[^{124}I]iodo-2′-fluoro-2′-deoxy-1-β-D-arabino-5-iodouracil ([^{124}I]FIAU) (*15–17*) and with the acycloguanosine derivatives 8-[^{18}F]fluoro-9-[[2-hydroxy-1-(hydroxymethyl)ethoxy]methyl]guanine([^{18}F]GCV) (*18,19*), 8-[^{18}F]fluoro-9-[4-hydroxy-3-(hydroxymethyl)-1-butyl]guanine ([^{18}F]PCV) (*13,20,21*), and 9-[4-[^{18}F]fluoro-3-(hydroxymethyl)butyl]guanine ([^{18}F]FHBG) (*10,14,22*) has been shown. Our primary studies used [^{18}F]GCV for imaging the expression of the wild-type HSV1-tk gene in living mice (*10–12,18,19,23,24*). In an attempt to improve the properties of this enzyme/substrate-based PRG/PRP system, we investigated a mutant HSV1-tk gene (HSV1-sr39tk) encoding an enzyme that leads to higher intracellular accumulation of [^{18}F]GCV and its carba-analog, [^{18}F]PCV (*20*). We also investigated [^{18}F]PCV (*25*) and showed that it improved the sensitivity for imaging the expression of HSV1-tk in living mice (*21*). Meanwhile, Alauddin et al. (*26*) reported the synthesis and preliminary in vitro evaluation of another [^{18}F]fluorine-radiolabeled analog of penciclovir, [^{18}F]FHBG, and later evaluated its accumulation to subcutaneous tumors in nude mice (*22*). We recently reported that [^{18}F]FHBG and [^{14}C]FIAU are superior to [^{18}F]PCV as PRPs for monitoring HSV1-tk PRG expression in vitro (*27*), and our most recent imaging studies in mice show low background accumulation and relatively high sensitivity with [^{18}F]FHBG (*10,14*). The fact that [^{18}F]FHBG exhibits better sensitivity in our mouse imaging studies and the fact that [^{18}F]FHBG can be synthesized at high specific activities prompted us to characterize the pharmacokinetics of [^{18}F]FHBG in humans.

[^{18}F]FHBG is a side-chain [^{18}F]fluorine-radiolabeled analog of the antiviral drug penciclovir. Our goal in this study was to characterize the biodistribution and route of clearance of [^{18}F]FHBG in healthy human volunteers. We also analyzed the stability of [^{18}F]FHBG and the blood cell–plasma partition of [^{18}F]FHBG, and we determined from the images, by region-of-interest (ROI) analysis, the time–activity curve of [^{18}F]FHBG to assess its radiation safety in imaging humans. Finally, blood and urine pharmacologic tests were performed to confirm that the [^{18}F]FHBG tracer is not toxic.

MATERIALS AND METHODS

Synthesis of [^{18}F]FHBG Precursor

p-Toluenesulfonyl chloride (350 mg, 1.8 mmol) was added to a solution of N^2-(*p*-anisyldiphenylmethyl)-9-[(4-hydroxy)-3-*p*-anisyldiphenylmethoxymethylbutyl]guanine (*26*) (250 mg, 0.31 mmol) in 5 mL pyridine, and the reaction mixture was stirred at room temperature for 3 h. Ethyl acetate (35 mL) was added, and the solution was washed with water (2 × 30 mL). The aqueous layer was further extracted with ethyl acetate (35 mL). The combined organic layers were dried (Na_2SO_4), concentrated, and purified by silica gel chromatography (3:97 CH_3OH:CH_2Cl_2) to yield the title product (112 mg, 37%). The product was further purified by semipreparative high-performance liquid chromatography (HPLC) (Adsorbosphere HS [Alltech Associates, Inc., Deerfield, IL], silica, 5 μm, 10 × 500 mm, 3.0 mL/min flow rate, 254-nm ultraviolet detector, with an eluent of 3% CH_3OH in CH_2Cl_2). The retention time for the product under these conditions was 13 min, and 88 mg of the pure product were obtained. ^{1}H nuclear magnetic resonance data (360 MHz; $CDCl_3$) are as follows: 1.54–1.70 (m, 3H, 2′H and 3′H), 2.42 (s, 3H, CH_3), 2.92–3.05 (m, 2H, 5′H), 3.55–3.62 (m, 2H, 1′H), 3.73 (s, 3H, CH_3O), 3.76 (s, 3H, CH_3O), 3.93–4.08 (m, 2H, 4′H), 6.74–7.02 (m, 4H, aromatic), 7.13–7.36 (m, 27H, aromatic and C_8H), and 7.73 (d, J = 7.9 Hz, 2H, aromatic). These nuclear magnetic resonance data are consistent with values reported in the literature (*26*).

Synthesis and Purification of [^{18}F]FHBG

No-carrier-added [^{18}F]fluoride ion produced by irradiation of $H_2{}^{18}O$ with 11 MeV protons using an RDS 112 cyclotron (CTI, Knoxville, TN/Siemens Medical Systems, Inc., Hoffman Estates, IL) was delivered to a Pyrex (Corning Inc., Corning, NY) glass reaction vessel containing potassium carbonate (0.75 mg) and Kryptofix 2.2.2 (10 mg; Aldrich, Milwaukee, WI) dissolved in water (0.04 mL) and CH_3CN (0.75 mL). The solution was evaporated at 115°C by bubbling nitrogen gas through it, and the residue was dried by azeotropic distillation with acetonitrile (3 × 0.5 mL). To this anhydrous residue was added a solution of N^2-(*p*-anisyldiphenylmethyl)-9-[(4-tosyl)-3-*p*-anisyldiphenylmethoxymethylbutyl]guanine (3–4 mg) in dry dimethyl sulfoxide (0.8 mL). The reaction mixture was heated for 20 min at 150°C in an oil bath. The solution was cooled, diluted with 4 mL water, and passed through a C_{18} Sep-Pak column (Waters, Milford, MA) activated previously by flushing 5 mL CH_3OH followed by 10 mL deionized water. The column was eluted with water (3 × 4 mL), and the aqueous eluents were discarded. The product was subsequently eluted with CH_3OH (2 mL). The methanolic solution was acidified with 0.4 mL 1N HCl and concentrated to 0.8 mL at 100°C with a stream of nitrogen gas. The solution was cooled, partially neutralized with 0.18 mL 1N NaOH, and diluted with the HPLC mobile phase (1.3 mL). The crude product was injected onto a C-18 semipreparative HPLC column ([Phenomenex Inc., Torrance, CA] 5 μm, 10 × 250 mm, 5.0 mL/min flow rate, with a mobile phase of 50 mmol/L NH_4OAc:C_2H_5OH = 93:7). Pure [^{18}F]FHBG, eluted off the column with a retention time of 15 min, was passed through an alumina Sep-Pak to remove any traces of [^{18}F]fluoride ion. The product was made isotonic with sodium chloride and passed through a 0.22-μm membrane filter into a sterile multidose vial. The product was found to be >99% radiochemically and chemically pure as determined by analytic HPLC (Econosil C-18 [Alltech], 5 μm, 4.6 × 250 mm, 1.0 mL/min flow rate, 254-nm ultraviolet and radioactivity detectors, with a mobile phase of 50 mmol/L NH_4OAc:CH_3CN = 90:10). The retention time for [^{18}F]FHBG under analytic HPLC conditions was 9 min. Radiochemical yield ranged from 6% to 13% (end of synthesis; corrected for decay). Thus, starting typically with 18,500 MBq [^{18}F]fluoride ion, 555–1,147 MBq product, ready for injection, were routinely obtained in 95–100 min. The specific activity of the

product was estimated to be >37,000 GBq/mmol. The final product was tested for sterility and pyrogenicity by standard technique (*28*) and found to be sterile and free from pyrogens.

Volunteers

Ten healthy volunteers (5 women, 5 men; age range, 20–39 y; mean age, 31 y) (Table 1) were recruited through newspaper advertisement. Informed consent was obtained as dictated by an approved protocol of the University of California, Los Angeles (UCLA), Human Subject Protection Committee. Before the start of the experiments, all volunteers were asked to urinate and female volunteers were asked to use an early pregnancy test to confirm lack of pregnancy. Each volunteer's body temperature was monitored throughout the study. For 5 of the volunteers, electrocardiography (ECG) findings and blood pressure were monitored before injection of the tracer and at the end of the study. Furthermore, blood and urine samples were collected from the same 5 volunteers before injection of [^{18}F]FHBG and at the end of the study to examine the pharmacologic and toxicologic parameters of the tracer.

PET Imaging Procedure

An ECAT EXACT HR+ PET scanner (CTI/Siemens) was used for all imaging, and there were 2 sets of protocols. For 3 volunteers (subjects 3–5; Table 1), the protocol began with a transmission scan acquired for 7.5 min per bed position (4 bed positions) using 3 rotating ^{68}Ge rod sources, each with approximately 88.8 MBq ^{68}Ge. Next, these volunteers received a bolus intravenous injection of the [^{18}F]FHBG tracer (99.9–225.7 MBq). The injection of [^{18}F]FHBG was followed 5 min later by 4 consecutive 2-dimensional 30-min emission scans (4 bed positions, 7.5 min per position) covering a field of view from above the heart to below the bladder, the same as for the transmission scan. A final whole-body (6 or 7 bed positions, 5 min per position) emission data acquisition covering the area from the head to the upper thighs was then performed after bladder voiding. For the last 5 volunteers (subjects 6–10; Table 1), a different imaging protocol was used to improve the quality of the results. First, a transmission scan was acquired for 3.2 min per bed position (7 bed positions) before a bolus injection (during 30 s) of the [^{18}F]FHBG tracer (114.7–229.4 MBq). The injection of [^{18}F]FHBG was followed 5 min later by 4 consecutive 35-min emission scans (7 bed positions, 5 min per position) covering the area from above the brain to the upper thighs. These volunteers were instructed to urinate immediately after the final emission scan. All images were acquired by moving the bed out of the scanner, after scanning each bed position, such that the lowest body part scanned was the first bed position. For all volunteers, at various times (approximately 1, 3, 5, and then every subsequent 30 min) after injection of the tracer, 3-mL blood samples were collected for whole-blood and plasma time–activity measurements. These blood samples were collected after heating the volunteer's hand to arterialize the venous blood. The plasma was separated from whole-blood samples and was counted along with whole blood in a NaI well counter (COBRA II; Packard Instrument Co., Meriden, CT). The counting efficiency of the well counter was 57% (determined using a standard of known amount of activity based on the dose calibrator). Two of the 10 volunteers (subjects 1 and 2; Table 1) did not have a complete dynamic set of emission data and were not included in dosimetry analysis.

Image Analysis and Dosimetry

Raw positron emission data were reconstructed using the ordered-subsets expectation maximization (OSEM) algorithm in the transaxial format with segmented attenuation correction (*29*,*30*). All reconstructions and image analysis used CAPP software, version 7.1 (CTI/Siemens). Two-dimensional views were assembled with bed position overlap and smoothed with a gaussian kernel of 10-mm full width at half maximum. All OSEM reconstructions were performed with 1 iteration and 30 subsets. The images were attenuation corrected using the transmission data collected over the same region of emission imaging. Transaxial images were resliced into coronal views.

ROIs were drawn over major organs (bladder, kidneys, gut, liver, heart), and the total organ activity at 4 scan times after the injection of [^{18}F]FHBG was estimated using the cylinder calibration factor. An experienced investigator drew the ROI such that the entire organ was included. To determine the biologic clearance of [^{18}F]FHBG, the activity was decay corrected back to the injection time and time–activity curves were obtained. For dosimetry analysis, time–activity curves were constructed using whole-organ activities at the scan time. For all organs except the bladder and intestines, the residence times, in hours, were calculated by dividing the area under the time–activity curves by the injected dose. The dynamic bladder model in the MIRD 3.0 program (*31*) was used to figure out the residence time for the bladder at various voiding intervals. The International Commission on Radiological Protection (ICRP) 30 gastrointestinal tract model in the MIRD

TABLE 1
Demographics of Study Participants

Subject no.	Sex	Age (y)	Height (cm)	Weight (kg)	Injected activity (MBq)
1	F	39	160.0	72.7	74.444
2	M	32	180.3	81.8	68.524
3	F	38	162.6	59.1	123.617
4	M	32	172.7	81.8	224.220
5	M	23	165.1	106.8	98.494
6	F	20	172.7	59.0	217.745
7	M	31	175.3	83.2	228.068
8	F	28	162.5	77.2	167.610
9	M	30	165.1	61.3	217.227
10	F	35	170.2	68.2	114.367
Mean		31	168.7	75.1	153.439
Range		20–39	160.0–180.3	59.0–106.8	68.524–228.068

program was used to determine the residence times in the small intestine, lower large intestine, and upper large intestine. Absorbed radiation doses by all organs were then calculated by the MIRD program.

^{18}F Cylinder and Determination of Calibration Factor

To obtain an accurate factor for converting ECAT counts to kBq of activity, an ^{18}F cylinder was imaged with the PET scanner. The cylinder had a base of 11-cm radius and a height of 16.5 cm. A volume of 6,283 mL water was mixed with 76.22 MBq [^{18}F]FDG and poured inside the cylinder. A transmission scan of 3.2 min per bed position was acquired, covering the entire cylinder with 2 bed positions. Next, 4 consecutive emission scans of 5 min per bed position (2 bed positions) were acquired. Cylinder emission data were reconstructed into a coronal image of the cylinder using the same method as for patient image reconstructions. An ROI was drawn over the entire PET image of the cylinder, and the total counts per second in the cylinder at each time point of the emission scan was determined. The total counts per second were decay corrected back to the time when the 76.22 MBq FDG had been measured with the dose calibrator. One count per second was found to be equivalent to 3,015.5 kBq. Also, 1 voxel was equivalent to 0.136 cm^3.

Urine Collection and HPLC Analysis

Fifty microliters of 1.5 mol/L $HClO_4$ were added to 500 μL of the urine sample collected from the volunteers at the end of the study (approximately 2 h after [^{18}F]FHBG injection). The solution was mixed and centrifuged at 11,000 rpm for 1 min. The supernatant was neutralized with 1N KOH and centrifuged. The supernatant was then transferred to a 0.2-μm MicroSpin filter (Alltech) and centrifuged again to remove any particulate matter. A 100- to 150-μL aliquot was injected onto the HPLC column (Partisil 10 SAX; Whatman, Ann Arbor, MI). The column was eluted with a linear KH_2PO_4 gradient, 0.01–1.0 mol/L (pH 3.7, at a flow rate of 1 mL/min), and the eluents were monitored with an ultraviolet detector (254 nm). One-milliliter fractions of the radioactive eluents were collected every minute for up to 30 min and counted in a COBRA II NaI well counter.

Statistical Analysis

Data on laboratory values are shown in Table 2. Values are expressed as mean ± SD. *t* tests were performed to further compare the values before injection with the values after injection. The null hypothesis was that they differ. Because 5 volunteers were tested, the number of degrees of freedom was 8. Assuming $P < 0.05$, a significant difference existed if the *t* value exceeded 2.306. *t* tests were also performed to determine whether any significant changes in temperature, blood pressure, or ECG measurements occurred.

RESULTS

Biosafety

The average body temperature across all volunteers was 36.9°C (SD, 0.37°C), and no significant change ($P < 0.05$) was observed after the injection of [^{18}F]FHBG ($n = 10$). There were also no significant changes ($P < 0.05$) in the systolic (before, 115.6 ± 16.4 mm Hg; after, 120.2 ± 10.0 mm Hg) and diastolic (before, 68.8 ± 11.7 mm Hg; after, 71.4 ± 11.2 mm Hg) blood pressures after injection of [^{18}F]FHBG ($n = 5$; 114.7–229.4 MBq). The ECG findings of the 5 volunteers before injection of [^{18}F]FHBG and at the end of the study were generally normal. The only exception was a single volunteer (subject 6; Table 1) who, before injection of [^{18}F]FHBG, had abnormal ECG findings (ectopic atrial rhythm), which improved after the injection.

Table 2 includes the urine and blood laboratory data, before and after injection of [^{18}F]FHBG, of the 5 volunteers for whom this information was obtained. Statistical analysis indicated that no significant changes ($P < 0.05$) in these blood and urine parameters were induced by injection of the [^{18}F]FHBG tracer, except for percentage of monocytes. However, the change in the absolute number of monocytes was not significant ($t = 0.3015$). Furthermore, in every volunteer, the percentage of monocytes was in the reference range before and after injection of [^{18}F]FHBG. Another noticeable change was in the platelet count of subject 10 (Table 1). The count increased from an abnormal level of 59,000/μL before injection to a normal level of 189,000/μL within 2 h after injection. However, overall, the average change in platelet counts across all volunteers was not significant.

Biodistribution and Dosimetry

Figure 1 is a dynamic coronal image set of the 4 whole-body emission images acquired (for subject 8) during 4 intervals after injection of [^{18}F]FHBG. Areas of highest activity are the bladder, kidneys, gut, and liver, illustrating the hepatobiliary and renal routes of [^{18}F]FHBG excretion. The percentage injected dose per gram of activity in the organs involved in the clearance pathway and some background organs for this volunteer are listed in Table 3. [^{18}F]FHBG activity in the gallbladder is not visible in Figure 1 because of the close proximity of the gallbladder to the liver and the fact that the coronal images are the sum of 30 coronal planes (12- to 15-mm thickness per plane). Low background activity in the other tissues indicates low blood-pool activity and low retention of [^{18}F]FHBG in cells, which do not express HSV1-tk. Negligible activity in the brain points to the inability of [^{18}F]FHBG to cross the blood–brain barrier. Figure 2 shows the time–activity curves of various organs in the same volunteer. Figures 1 and 2 show decline of activity over time in the liver, kidneys, and other organs, with the exception of the bladder and intestines. The activities in both figures have been decay corrected to the time of injection; thus the figures illustrate biologic clearance of [^{18}F]FHBG into the bladder and intestines from the other regions of the body. [^{18}F]FHBG clearance into the bladder is rapid, with 52% of the injected activity accumulating in the bladder within 45 min after injection. Activity in the intestine either remains relatively constant (in 3 of the 8 volunteers) or gradually rises during the 2 h after injection of [^{18}F]FHBG. Rapid clearance of [^{18}F]FHBG from the blood circulation was also observed, as shown by the blood time–activity curve of subject 8 in Figure 3. When [^{18}F]FHBG was injected as a bolus (in <30 s), >90% of the

TABLE 2
Laboratory Values

Test	Before injection	Two hours after injection	*t* value
Urine			
Gravity	1.02 ± 0.00	1.02 ± 0.00	1.140570428
pH	6.00 ± 0.35	6.40 ± 1.03	0.825136997
Red blood cells	0.60 ± 0.89	0.40 ± 0.89	0.353553391
White blood cells	2.00 ± 2.74	0.80 ± 1.79	0.820303112
Squamous epithelium cells	1.00 ± 2.24	0.20 ± 0.45	0.784464541
Blood			
White blood cells (1,000/μL)	5.99 ± 1.63	7.04 ± 1.11	1.188356246
Red blood cells (1,000,000/μL)	4.58 ± 0.68	4.51 ± 0.70	0.166007059
Hemoglobin (g/dL)	13.36 ± 1.92	13.10 ± 2.16	0.201218140
Hematocrit (%)	39.08 ± 4.19	38.22 ± 4.86	0.299799012
Mean corpuscular volume (fL)	86.24 ± 10.01	85.62 ± 9.85	0.098720358
Mean corpuscular hemoglobin (pg)	29.48 ± 4.36	29.30 ± 4.15	0.066834652
Mean corpuscular hemoglobin concentration (g/dL)	34.10 ± 1.55	34.14 ± 1.45	0.042126273
RDW SD (fL)	41.06 ± 3.56	40.84 ± 3.83	0.094158207
RDW coefficient of variation (%)	13.10 ± 0.91	13.10 ± 0.96	0
Platelet count (1,000/μL)	246.80 ± 105.70	267.00 ± 46.91	0.390595127
Mean platelet volume (fL)	10.96 ± 0.89	10.38 ± 0.48	1.284141584
Neutrophil differential (%)	61.72 ± 6.32	61.52 ± 5.53	0.053251413
Lymphocyte differential (%)	27.28 ± 6.13	28.52 ± 4.90	0.353266318
Monocyte differential (%)	8.72 ± 0.58	7.28 ± 0.86	3.121595890
Eosinophil differential (%)	1.98 ± 1.04	2.30 ± 1.59	0.376496644
Basophil differential (%)	0.30 ± 0.20	0.38 ± 0.27	0.534522484
Absolute neutrophil count (1,000/μL)	3.76 ± 1.38	4.36 ± 0.99	0.789063958
Absolute lymphocyte count (1,000/μL)	1.60 ± 0.31	1.98 ± 0.33	1.890570661
Absolute monocyte count (1,000/μL)	0.52 ± 0.13	0.50 ± 0.07	0.301511345
Absolute eosinophil count (1,000/μL)	0.12 ± 0.08	0.14 ± 0.11	0.316227766
Absolute basophil count (1,000/μL)	0.00 ± 0.00	0.02 ± 0.04	1
Sodium (mmol/L)	137.40 ± 2.41	137.00 ± 2.12	0.278693206
Potassium (mmol/L)	3.98 ± 0.28	4.00 ± 0.39	0.092847669
Chloride (mmol/L)	103.10 ± 2.12	103.40 ± 1.95	0.310460210
CO_2 content (mmol/L)	24.60 ± 1.52	24.60 ± 2.30	0
Glucose (mg/dL)	89.20 ± 8.67	88.40 ± 15.79	0.099304205
Creatinine (mg/dL)	0.72 ± 0.16	0.68 ± 0.26	0.291729983
Urea nitrogen (mg/dL)	13.40 ± 4.39	12.00 ± 3.39	0.564076075
Total protein (g/dL)	6.74 ± 0.36	6.36 ± 0.34	1.696023002
Albumin (g/dL)	3.96 ± 0.38	3.86 ± 0.38	0.418121005
Total bilirubin (mg/dL)	0.56 ± 0.09	0.68 ± 0.19	1.264911064
Alkaline phosphatase (U/L)	55.00 ± 10.82	53.40 ± 9.18	0.252164007
Aspartate aminotransferase (U/L)	23.60 ± 5.50	21.60 ± 6.35	0.532246295
Alanine aminotransferase (U/L)	19.20 ± 9.86	19.20 ± 9.47	0
Calcium (mg/dL)	9.22 ± 0.58	8.98 ± 0.18	0.883452209

RDW = red cell distribution width.
Data are mean ± SD (n = 5).

PET probe cleared from the blood circulation within 30 min (remaining, 8.42% ± 4.76%; n = 9). The average ratio of [^{18}F]FHBG in plasma to [^{18}F]FHBG in whole blood for 6 blood collection times after injection of [^{18}F]FHBG is shown in Table 4. The average is listed for the 7 volunteers who received smooth bolus injections over 30 s. These data indicate low accumulation of [^{18}F]FHBG by blood cells.

To determine the maximum dose of [^{18}F]FHBG tracer that can be safely injected into a patient, we used the organ residence times of each individual to calculate his or her absorbed radiation dose. Table 5 lists the average absorbed radiation doses for all organs of 8 volunteers. The bladder received the highest absorbed doses ($9.42 \times 10^{-5} \pm 1.48 \times 10^{-5}$ Gy/MBq), reflecting rapid clearance of most of the injected [^{18}F]FHBG into the bladder and making it the limiting organ as far as concerns the amount of [^{18}F]FHBG that can be injected without exceeding 0.05 Sv per organ per year (Food and Drug Administration [FDA] regulation). However, the patient's voiding interval affects the radiation dose absorbed by the urinary bladder, and because the urinary bladder is the limiting organ, the patient's frequency of urinating will change the maximum dose of [^{18}F]FHBG that can be injected per year. The data shown are for a 1-h

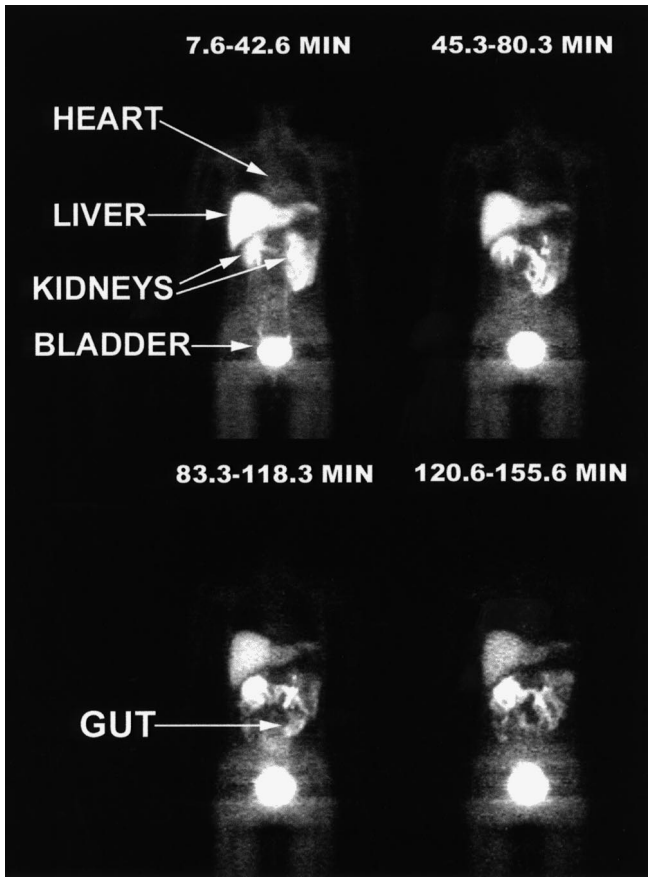

FIGURE 1. Whole-body coronal images of [^{18}F]FHBG biodistribution in healthy volunteer (subject 8) at 4 times after 167.6-MBq (4.53-mCi) intravenous injection of PET tracer. Images are sum of 30 coronal planes (12–15 mm thick per plane). [^{18}F]FHBG clears from other organs into intestines and bladder over time.

voiding interval. Using this voiding interval, a maximum of 530.8 MBq ($0.05/9.42 \times 10^{-5}$) [^{18}F]FHBG can be intravenously injected per year. The other major organs that receive relatively high doses are the small and large intestines, kidneys, and liver. On the other hand, the skin, breasts, brain, thymus, and testes absorb the lowest doses.

Stability of [^{18}F]FHBG

Figure 4 illustrates the stability of [^{18}F]FHBG in the urine approximately 2.5 h after injection ($n = 10$; 70.3–229.4 MBq). When the urine sample is analyzed on an anion exchange HPLC column, undegraded [^{18}F]FHBG is eluted at approximately 5–6 min (determined by running pure [^{18}F]FHBG through the same type of anion exchange column and then observing the time of elution). On the basis of this analysis, 82.94% ± 9.31% ($n = 10$) of the total activity found in the urine specimens was stable [^{18}F]FHBG, hinting at the biostability of [^{18}F]FHBG.

DISCUSSION

This phase I study shows the safety of, and absence of toxicity from, intravenously injected [^{18}F]FHBG tracer. Lack of a significant rise in body temperature verifies that [^{18}F]FHBG is nonpyrogenic. [^{18}F]FHBG tracer did not have a significant effect on the volunteers' blood pressures, and ECG findings remained normal after tracer injection. Furthermore, [^{18}F]FHBG did not cause any significant changes in blood and urine parameters, supporting its lack of toxicity or pharmacologic effects. Finally, dosimetry calculations indicated acceptable absorbed doses by critical organs and even lower absorbed doses by radiation-sensitive organs.

We did not expect pharmacologic toxicity from tracer doses of [^{18}F]FHBG, and our main safety concern was to keep the absorbed radiation doses below the limit (0.05 Sv per year) set by the FDA. Taking into account a specific activity of 37,000 GBq/mmole, the highest whole-blood concentration of [^{18}F]FHBG observed (subject 7; Table 1) 1 min after injection was approximately 1.5 nmole/L. That is approximately 160,000-fold less than the blood concentration reached when a single dose of ganciclovir (5 mg/kg) is administered for suicide gene therapy in cancer patients with malignant mesothelioma (*32*).

The limiting organ (bladder) defined the maximum single injected dose to be 530 MBq with a 1-h voiding interval, using the limit of 0.05 Gy to the critical organ per year. At this injected level, the doses to the radiation-sensitive organs, such as the testes and ovaries, are well below the 0.03-Gy limit of the FDA. The average effective dose is 0.01588 ± 0.0033 mSv/MBq (0.5876 ± 0.1221 mSv/mCi). Assuming that a maximum of 530 MBq can be injected into a patient, using a 1-h voiding interval, that patient would be exposed to 8.42 mSv of effective dose. This corresponds to risk category IIb as defined by the ICRP (*33*). ICRP defines category IIb as a minor to intermediate level of risk, appropriate for intermediate to moderate societal benefit. The 95% confidence interval for the average effective dose is 0.0131–0.0186 mSv/MBq (0.4853–0.6887 mSv/mCi). At

TABLE 3
Percentage Injected Dose [^{18}F]FHBG per Gram for Subject 8

Time (min)	Bladder	Intestine	Heart	Head and neck	Liver	Kidney
7.6	0.00971	0.00150	0.00085	0.0001530	0.00303	0.00402
45.3	0.01778	0.00159	0.00051	0.0001030	0.00205	0.00225
83.3	0.02080	0.00216	0.00038	0.0000751	0.00167	0.00164
120.6	0.02297	0.00258	0.00030	0.0000572	0.00134	0.00157

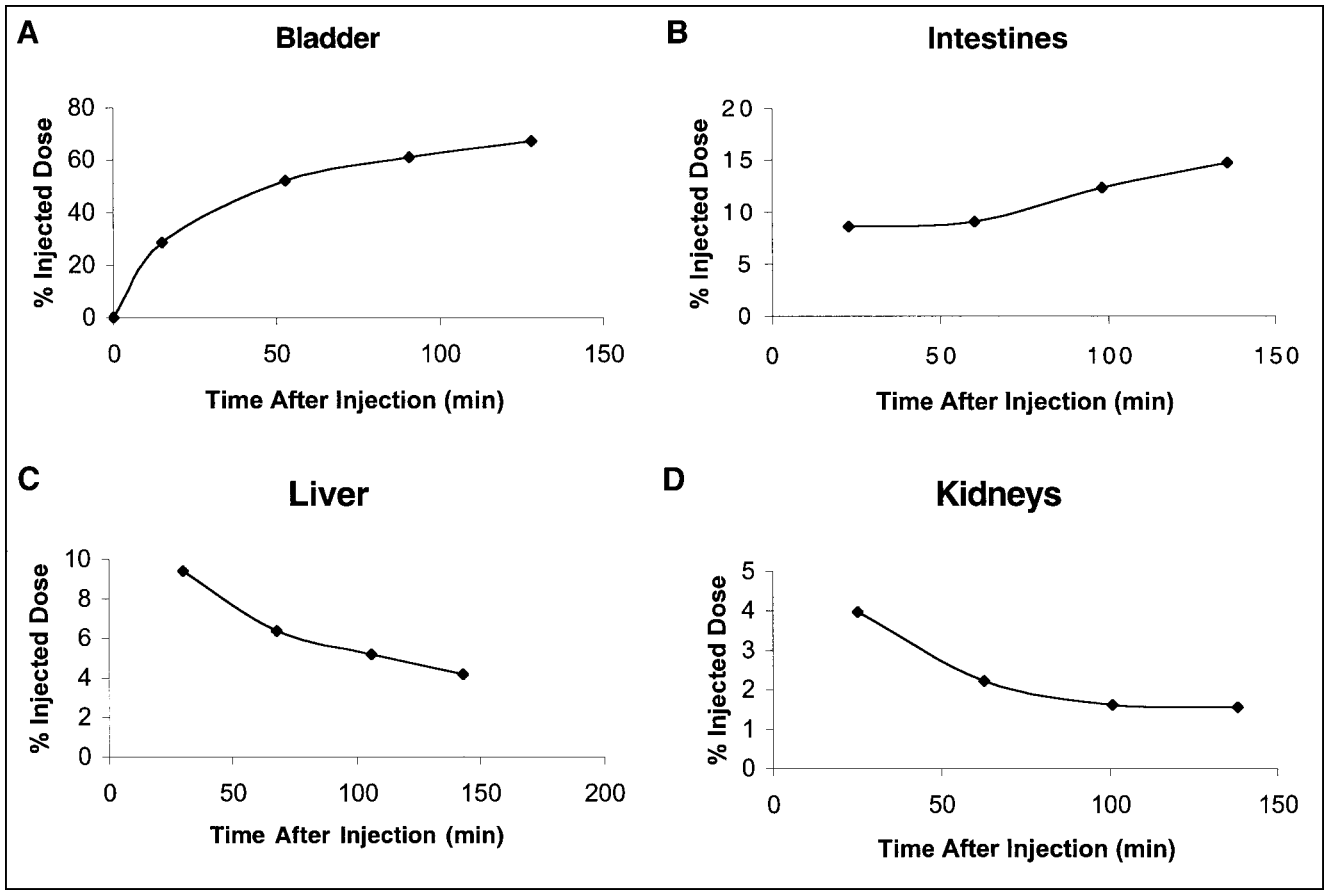

FIGURE 2. Time–activity curves of [^{18}F]FHBG in bladder (A), intestines (B), liver (C), and kidneys (D) of healthy volunteer (subject 8). Activities were decay corrected to time of injection; graphs indicate biologic clearance of [^{18}F]FHBG into bladder and intestines and out of liver and kidneys. Graphs indicate percentage of total injected activity in each organ versus time after injection of [^{18}F]FHBG tracer.

the maximum of this confidence interval, a 530-MBq injected dose with a 1-h voiding interval would expose the patient to 9.86 mSv of effective dose, which is still in category IIb. Therefore, the variations in effective doses were small and eliminate the need to examine more volunteers.

The biodistribution of intravenously injected [^{18}F]FHBG showed that its route of clearance is through the renal and hepatobiliary pathways. The minor [^{18}F]FHBG activity observed in the heart on the first scan (approximately 30 min after injection) cleared biexponentially. The amount of [^{18}F]FHBG in the liver and kidneys was initially higher, but [^{18}F]FHBG clearance from those organs was also rapid (Fig. 2). The gallbladder was clearly visible in some (but not all)

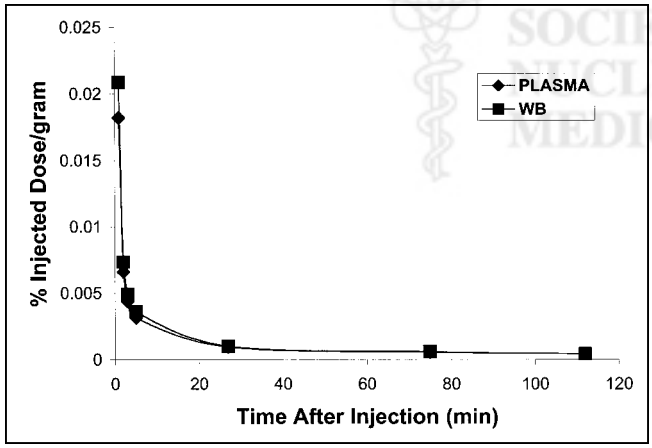

FIGURE 3. Time–activity curve of [^{18}F]FHBG in whole blood (WB) and plasma of healthy volunteer (subject 8). [^{18}F]FHBG is removed from blood rapidly, and most activity is in plasma portion. Average ratio of activity in plasma to activity in whole blood during approximately 2 h after tracer injection was 0.888 for this person.

TABLE 4
Ratio of [^{18}F]FHBG in Plasma to [^{18}F]FHBG in Whole Blood

Subject no.	Mean	SD
4	0.924	0.07582
5	0.948	0.07825
6	0.968	0.06248
7	0.888	0.06788
8	0.911	0.03976
9	0.873	0.09291
10	0.878	0.34954
Mean	0.9128571	
SD	0.0361129	

TABLE 5
Dosimetry Data

Target organ	Mean dose*		SD		Primary contribution
	rad/mCi	mGy/MBq	rad/mCi	mGy/MBq	
Adrenals	0.0317	0.00855	0.0086	0.00233	Remainder of body
Brain	0.0155	0.00418	0.0031	0.00084	Remainder of body
Breasts	0.0153	0.00415	0.0026	0.00070	Remainder of body
Gallbladder wall	0.0542	0.01465	0.0310	0.00840	Remainder of body
Lower large intestine wall	0.0700	0.01891	0.0184	0.00494	Lower large intestine
Small intestine	0.1550	0.04193	0.0541	0.01462	Small intestine
Stomach	0.0281	0.00758	0.0057	0.00155	Remainder of body
Upper large intestine wall	0.1689	0.04566	0.0574	0.01551	Upper large intestine
Heart wall	0.0303	0.00818	0.0065	0.00177	Heart content
Kidneys	0.1890	0.05109	0.1281	0.03455	Kidneys
Liver	0.0826	0.02230	0.0295	0.00796	Liver
Lungs	0.0201	0.00542	0.0040	0.00107	Remainder of body
Muscle	0.0214	0.00579	0.0051	0.00138	Remainder of body
Ovaries	0.0502	0.01358	0.0112	0.00303	Remainder of body
Pancreas	0.0312	0.00843	0.0071	0.00192	Remainder of body
Red marrow	0.0252	0.00681	0.0046	0.00125	Remainder of body
Bone surfaces	0.0217	0.00586	0.0037	0.00100	Remainder of body
Skin	0.0151	0.00408	0.0024	0.00066	Remainder of body
Spleen	0.0265	0.00716	0.0069	0.00187	Remainder of body
Testes	0.0206	0.00556	0.0025	0.00069	Remainder of body
Thymus	0.0184	0.00498	0.0032	0.00087	Remainder of body
Thyroid	0.0159	0.00430	0.0025	0.00069	Remainder of body
Urinary bladder wall	0.3488	0.09424	0.0548	0.01476	Urinary bladder
Uterus	0.0542	0.01464	0.0083	0.00223	Remainder of body
Total body	0.0259	0.00700	0.0055	0.00150	Remainder of body
Effective dose equivalent†	0.0784	0.02118	0.0186	0.00503	Remainder of body
Effective dose†	0.0587	0.01588	0.0122	0.00330	Urinary bladder

*n = 8.
†In units of rem/mCi or mSv/MBq.

individuals, with the amount of [^{18}F]FHBG generally increasing over time. The amount of tracer in the gut either remained constant or increased slightly over time, perhaps reflecting the biliary excretion of [^{18}F]FHBG. The average maximum [^{18}F]FHBG activity that accumulated in the gut of the volunteers (n = 8) during the studies was 9.2% ± 3.0% of the injected dose. The background activity in the other organs was very low to negligible and decreased with time. Penetration of [^{18}F]FHBG across the blood–brain barrier was not observed. [^{18}F]FHBG cleared rapidly into the bladder within the first hour after intravenous bolus injection, and the amount of [^{18}F]FHBG within the bladder continued to increase throughout scanning. The average maximum [^{18}F]FHBG activity that accumulated in the bladder of the volunteers (n = 8) during the studies was 65.3% ± 8.7% of the injected dose. Therefore, the intensity of the [^{18}F]FHBG signal in and around the bladder always remained high.

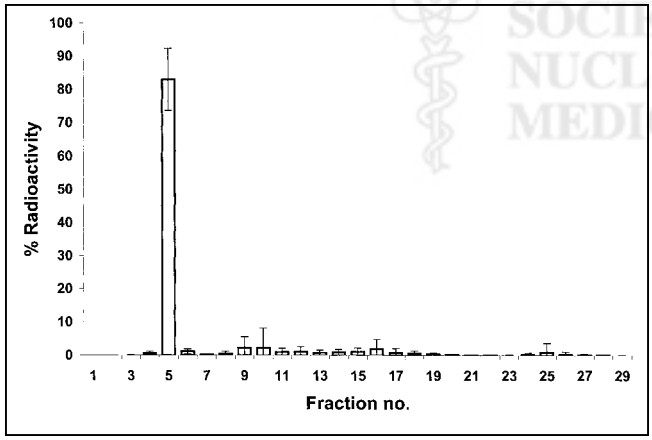

FIGURE 4. Percentage of stable [^{18}F]FHBG found in urine samples of healthy volunteers 2.5 h after injection of [^{18}F]FHBG tracer. [^{18}F]FHBG elutes from anion exchange column at 6 min. This analysis shows that 82.94% ± 9.31% (n = 10) of total activity found in urine specimens was stable [^{18}F]FHBG.

On the basis of these patterns of biodistribution, we believe that imaging of the HSV1-tk gene with [^{18}F]FHBG should be possible everywhere except the lower abdomen (because of high bladder activity and increasing intestinal activity) and central nervous system (because of restricted passage of [^{18}F]FHBG across the blood–brain barrier). Imaging near the bladder may be possible if the bladder is irrigated; this will require further testing. We are also testing bradykinin drugs (*34*) in mouse models, which may make

possible the uptake of [^{18}F]FHBG into the brain. Furthermore, lesions that disrupt the blood–brain barrier will provide access for [^{18}F]FHBG. We recommend that a 1-h wait be allowed after intravenous injection so that background activity can decline sufficiently for effective imaging of low levels of HSV1-tk expression. Within the first hour, activity in the liver and kidneys may be too high for HSV1-tk signal to be distinguished from background signal in those areas. Activity in the liver is halved 1 h after tracer injection (Fig. 2; Table 3). It may also be possible to wait longer before imaging HSV1-tk expression in the liver. Furthermore, HSV1-tk expression in liver cells should lead to [^{18}F]FHBG retention within the liver through time; thus, dynamic imaging of the liver may also be helpful.

Before undergoing imaging at 1 h, patients should be asked to urinate completely. As long as the 530-MBq limit per year is not exceeded, a patient may be scanned as many times as needed. The required injected dose of [^{18}F]FHBG may depend on the particular application. In our study, as few as 74 MBq were used to obtain emission images for up to 2.5 h. For most patients who require repeated scanning to monitor gene expression, up to 7 scans at 74 MBq per scan can be performed with a 1-h voiding interval. It may be possible to increase the amount of [^{18}F]FHBG given using irrigation or more frequent bladder voiding. In fact, if the patient can void every half hour, bladder exposure will be reduced to $5.0 \times 10^{-5} \pm 7.6 \times 10^{-6}$ Gy/MBq, which raises the allowed dose per year to 1,000 MBq.

Almost negligible entrapment of [^{18}F]FHBG in tissues that are not involved in its metabolism or clearance, and rapid [^{18}F]FHBG blood clearance, result in a suitable background activity in those tissues. For example, we see a potential for imaging HSV1-tk expression in mesothelioma patients undergoing HSV1-tk/GCV gene therapy (*32*). However, there is a concern that fast clearance will not allow [^{18}F]FHBG sufficient time to be trapped by the HSV1-TK enzyme. Our ongoing studies in mice indicate that the kinetics of HSV1-tk and its mutant subtype HSV1-sr39tk cause sufficient entrapment of [^{18}F]FHBG to yield activity distinguishable from the background in PET images. In fact, we have also shown imaging of HSV1-sr39tk expression in tumor xenografts, liver, and muscle in nude mice (*13,14*).

A variety of applications can be foreseen for the [^{18}F]FHBG tracer. [^{18}F]FHBG imaging in targeted suicide gene therapy of cancer with wild-type HSV1-tk may aid in the correct targeting of the suicide transgene to cancer cells and show the distribution and expression from a variety of vectors delivering the HSV1-tk gene. [^{18}F]FHBG may also provide the means to track the biodistribution, as well as the magnitude and duration of expression of a therapeutic transgene, linked to the PRG wild-type HSV1-tk (*35*) or a higher affinity HSV1-tk mutant, HSV1-sr39tk (*13,14*). Another application of [^{18}F]FHBG may be the detection of viral infections, such as HSV1, cytomegalovirus (CMV), varicella zoster virus, and hepatitis B virus. [^{18}F]FHBG is an analog of penciclovir, which has been shown to be a selective inhibitor of replication of these viruses (*36–39*) in various degrees; our positron-labeled penciclovir analog might be phosphorylated by the viral thymidine kinases. If phosphorylated, [^{18}F]FHBG will be trapped inside the cells infected by these viruses and can be used as a probe for diagnostic imaging and localization of the infection.

[^{18}F]FHBG imaging of viral infections needs to be performed while the viruses are actively replicating, because trapping of [^{18}F]FHBG requires production of viral thymidine kinase. Furthermore, [^{18}F]FHBG does not pass through the blood–brain barrier and may not detect neuronal infections. Viral infections in the central nervous system will be detected only if the blood–brain barrier is disrupted by the infection. Unfortunately, imaging with [^{18}F]FHBG will not be effective in the detection of gastrointestinal CMV infections, which are hard to diagnose by conventional means, unless the signal from the infection exceeds the relatively high background activity around the intestines. However, after an hour the background activity in the liver may be reduced enough to reveal [^{18}F]FHBG trapping inside virally infected hepatocytes. [^{18}F]FHBG may also be useful in detecting HSV1 eye infections and CMV retinitis. Although imaging of HSV1 outbreaks on the skin may not be clinically useful, [^{18}F]FHBG imaging of patients with such skin lesions can serve as a preliminary proof of principal. The clinical utility of imaging with 2′-fluoro-5-methyl-1-β-D-arabinosyluracil (a pyrimidine nucleoside analog) for the detection of HSV encephalitis has been suggested by autoradiographic studies in a rat model (*40*). [^{18}F]FHBG may also be a good tracer for detecting HSV encephalitis and may be useful for investigating viral replication in neuronal ganglions.

CONCLUSION

[^{18}F]FHBG is a safe tracer with highly desirable pharmacokinetic properties. Its rapid clearance and low background activity make it suitable for imaging HSV1-tk gene expression in all regions except the brain and, possibly, the lower abdomen. [^{18}F]FHBG has shown high affinity for HSV1-tk in cell culture and animal studies and is now ready for testing on patients who express HSV1-tk.

ACKNOWLEDGMENT

The authors thank Ron Sumida, Larry Pang, Francine Aguilar-Meadors, Priscilla Contreras, Sumon Wongpiya, and Cindy Lim for technical assistance and Dr. Tatsushi Toyokuni and Mankit Ho for routine synthesis of [^{18}F]FHBG. The authors also acknowledge the UCLA cyclotron crew for outstanding support and, finally, are grateful for the participation of the 10 volunteers in this research project. This study was supported in part by an intramural grant from the UCLA Gene Therapy Program.

REFERENCES

1. Springer CJ, Niculescu-Duvaz I. Prodrug-activating systems in suicide gene therapy. *J Clin Invest.* 2000;105:1161–1167.
2. Lal S, Lauer UM, Niethammer D, Beck JF, Schlegel PG. Suicide genes: past, present and future perspectives. *Immunol Today*. 2000;21:48–54.
3. Malkowicz BS, Johnson OJ. Gene therapy for prostate cancer. *Hematol Oncol Clin North Am.* 1998;12:649–664.
4. Sterman DH, Kaiser LR, Albelda SM. Gene therapy for malignant pleural mesothelioma. *Hematol Oncol Clin North Am.* 1998;12:553–568.
5. Adams SW, Emerson SG. Gene therapy for leukemia and lymphoma. *Hematol Oncol Clin North Am.* 1998;12:631–648.
6. Alavi JB, Eck SL. Gene therapy for malignant gliomas. *Hematol Oncol Clin North Am.* 1998;12:617–629.
7. Smith MJ, Rousculp MD, Goldsmith KT, Curiel DT, Garver RI Jr. Surfactant protein A-directed toxin gene kills lung cancer cells *in vitro*. *Hum Gene Ther*. 1994;5:29–35.
8. Vile RG, Hart IR. Use of tissue-specific expression of the herpes simplex virus thymidine kinase gene to inhibit growth of established murine melanomas following direct intratumoral injection of DNA. *Cancer Res.* 1993;53:3860–3864.
9. Vandier D, Rixe O, Brenner M, Gouyette A, Besnard F. Selective killing of glioma cell lines using an astrocyte-specific expression of the herpes simplex virus-thymidine kinase gene. *Cancer Res.* 1998;58:4577–4580.
10. Gambhir SS, Herschman HR, Cherry SR, et al. Imaging transgene expression with radionuclide imaging technologies. *Neoplasia*. 2000;2:118–138.
11. Herschman HR, MacLaren DC, Iyer M, et al. Seeing is believing: non-invasive, quantitative and repetitive imaging of reporter gene expression in living animals, using positron emission tomography. *J Neurosci Res.* 2000;59:699–705.
12. Gambhir SS, Barrio JR, Herschman HR, Phelps ME. Assays for noninvasive imaging of reporter gene expression. *Nucl Med Biol.* 1999;26:481–490.
13. Yu Y, Annala AJ, Barrio JR, et al. Quantification of target gene expression by imaging reporter gene expression in living animals. *Nat Med.* 2000;6:933–937.
14. Yaghoubi SS, Wu L, Liang Q, et al. Direct correlation between positron emission tomographic images of two reporter genes delivered by two distinct adenoviral vectors. *Gene Ther.* 2001;8:1072–1080.
15. Tjuvajev JG, Avril N, Oku T, et al. Imaging herpes virus thymidine kinase gene transfer and expression by positron emission tomography. *Cancer Res.* 1998;58:4333–4341.
16. Tjuvajev JG, Avril N, Safer M, et al. Quantitative PET imaging of HSV1-TK gene expression with [I-124]FIAU [abstract]. *J Nucl Med.* 1997;38(suppl):239P.
17. Dubrovin M, Hackman T, Ponomarev V, et al. Monitoring tumor gene therapy with cytosine deaminase and 5FC by imaging CD/HSV1-TK fusion gene expression with [^{124}I]-FIAU and PET [abstract]. *J Nucl Med.* 2000;41(suppl):80P.
18. Gambhir SS, Barrio J, Wu L, et al. Imaging of adenoviral directed herpes simplex virus type 1 thymidine kinase gene expression in mice with ganciclovir. *J Nucl Med.* 1998;39:2003–2011.
19. Gambhir SS, Barrio JR, Phelps ME, et al. Imaging adenoviral-directed reporter gene expression in living animals with positron emission tomography. *Proc Natl Acad Sci USA.* 1999;96:2333–2338.
20. Gambhir SS, Bauer E, Black ME, et al. A mutant herpes simplex virus type 1 thymidine kinase reporter gene shows improved sensitivity for imaging reporter gene expression with positron emission tomography. *Proc Natl Acad Sci USA.* 2000;97:2785–2790.
21. Iyer M, Barrio JR, Namavari M, et al. 8-[^{18}F]fluoropenciclovir: an improved reporter probe for imaging HSV1-tk reporter gene expression in vivo using PET. *J Nucl Med.* 2001;42:96–105.
22. Alauddin MM, Shahinian A, Gordon EM, Conti PS. Evaluation of F-18 9-(4-fluoro-3-hydroxymethylbutyl)guanine ([F-18]FHBG as a PET imaging agent for gene expression in tumor bearing nude mice [abstract]. *J Nucl Med.* 1999; 40(suppl):26P.
23. Gambhir SS, Barrio JR, Herschman HR, Phelps ME. Imaging gene expression: principles and assays. *J Nucl Cardiol.* 1999;6:219–233.
24. Gambhir SS. Imaging gene expression: concepts and future outlook. In: Schiepers C, ed. *Diagnostic Nuclear Medicine*. New York, NY: Springer-Verlag; 1999: 253–271.
25. Iyer M, Barrio JR, Namavari M, et al. 8-[^{18}F]Fluoropenciclovir: an improved reporter probe for imaging HSV1-tk reporter gene expression in vivo using PET. *J Nucl Med.* 2001;42:96–105.
26. Alauddin MM, Conti PS. Synthesis and preliminary evaluation of 9-(4-[^{18}F]-fluoro-3-hydroxymethylbutyl)guanine ([^{18}F]FHBG): a new potential imaging agent for viral infection and gene therapy using PET. *Nucl Med Biol.* 1998;25: 175–180.
27. Iyer M, Bauer E, Barrio JR, et al. Comparison of FPCV, FHBG, and FIAU as reporter probes for imaging herpes simplex virus 1 thymidine kinase reporter gene expression [abstract]. *J Nucl Med.* 2000;41(suppl):80P.
28. Williams CC, Borchert RD, Clanton JA. The bacterial endotoxin test in the PET facility. *J Nucl Med.* 1993;34:469–473.
29. Lonneux M, Borbath I, Bol A, et al. Attenuation correction in whole-body FDG oncological studies: the role of statistical reconstruction. *Eur J Nucl Med.* 1999;26:591–598.
30. Hudson HM, Larkin RS. Accelerated image reconstruction using ordered subsets of projection data. *IEEE Trans Med Imaging*. 1994;13:601–609.
31. Loevinger R, Budinger TF, Watson EE. *MIRD Primer for Absorbed Dose Calculations*. New York, NY: Society of Nuclear Medicine; 1991.
32. Sterman DH, Treat J, Litzky LA, et al. Adenovirus-mediated herpes simplex virus thymidine kinase/ganciclovir gene therapy in patients with localized malignancy: results of a phase I clinical trial in malignant mesothelioma. *Hum Gene Ther*. 1998;9:1083–1092.
33. *ICRP Publication 62: Radiological Protection in Biomedical Research*. Oxford, U.K.: Pergamon Press; 1991:12.
34. Bartus RT, Elliott P, Hayward N, Dean R, McEwen EL, Fisher SK. Permeability of the blood brain barrier by the bradykinin agonist, RMP-7: evidence for a sensitive, auto-regulated, receptor-mediated system. *Immunopharmacology*. 1996;33:270–278.
35. Tjuvajev JG, Joshi A, Callegari J, et al. A general approach to the non-invasive imaging of transgenes using cis-linked herpes simplex virus thymidine kinase. *Neoplasia*. 1999;1:315–320.
36. Korba BE, Malcolm RB. Penciclovir is a selective inhibitor of hepatitis B virus replication in cultured human hepatoblastoma cells. *Antimicrob Agents Chemother.* 1996;40:1282–1284.
37. Shaw T, Mok SS, Locarnini SA. Inhibition of hepatitis B virus DNA polymerase by enantiomers of penciclovir triphosphate and metabolic basis for selective inhibition of HBV replication by penciclovir. *Hepatology*. 1996;24:996–1002.
38. Zimmermann A, Michel D, Pavic I, et al. Phosphorylation of aciclovir, ganciclovir, penciclovir and S2242 by the cytomegalovirus UL97 protein: a quantitative analysis using recombinant vaccinia viruses. *Antiviral Res.* 1997;36:35–42.
39. Sacks SL, Straus SE, Whitely RJ, Griffiths PD. *Clinical Management of Herpes Virus*. Amsterdam, The Netherlands: IOS Press; 1995.
40. Saito Y, Rubenstein R, Price R, Fox J, Watanabe K. Diagnostic imaging of herpes simplex virus encephalitis using antiviral drug: autoradiographic assessment in animal model. *Ann Neurol.* 1984;15:548–558.

JNM The Journal of NUCLEAR MEDICINE

Human Pharmacokinetic and Dosimetry Studies of [^{18}F]FHBG: A Reporter Probe for Imaging Herpes Simplex Virus Type-1 Thymidine Kinase Reporter Gene Expression

Shahriar Yaghoubi, Jorge R. Barrio, Magnus Dahlbom, Meera Iyer, Mohammad Namavari, Nagichettiar Satyamurthy, Robin Goldman, Harvey R. Herschman, Michael E. Phelps and Sanjiv S. Gambhir

J Nucl Med. 2001;42:1225-1234.

The Journal of Nuclear Medicine is published monthly.
SNMMI | Society of Nuclear Medicine and Molecular Imaging
1850 Samuel Morse Drive, Reston, VA 20190.
(Print ISSN: 0161-5505, Online ISSN: 2159-662X)

SNMMI SOCIETY OF NUCLEAR MEDICINE AND MOLECULAR IMAGING